An *ab Initio* Study on the Oxidative Coupling of Methane over a Lithium-Doped MgO Catalyst: Surface Defects and Mechanism

Michael A. Johnson, Eugene V. Stefanovich,† and Thanh N. Truong*
Department of Chemistry, University of Utah, Salt Lake City, Utah 84112
Received: December 17, 1996[⊗]

We present a study on the catalytic cycle responsible for coupling of methane by molecular oxygen over a lithium-doped magnesium oxide catalyst. To elucidate the mechanism by which methyl radicals are produced and the active sites are regenerated, geometries and energies of relevant reaction intermediates were determined using an *ab initio* embedded cluster model. Our results suggest a new mechanism that requires only one active site and does not involve the energetically costly process of creating lattice vacancies. This mechanism is more consistent with the available experimental data than the Ito−Lunsford mechanism proposed earlier.

Introduction

Efficient utilization of methane, the primary component of natural gas, is becoming an immediate goal as we face issues of diminishing natural resources. Unfortunately, the remote locations of most natural gas reserves make transportation of this fuel economically unreasonable.[1] One means to exploit the remote gas sources is to first convert methane to more useful higher carbon products that can easily be transported to the consuming facility. However, existing methane conversion methods[2] have proven to be prohibitively expensive. Thus, developing a less expensive catalytic conversion method is of great interest and technological significance.

Numerous research efforts have been devoted to the design of efficient metal oxide catalysts for methane conversion with high selectivity to C_2 compounds and low operational temperatures (for review, see refs 1 and 3). Among these catalysts, lithium-doped magnesium oxide (Li/MgO) is of particular interest for several reasons. First, Li/MgO effectively converts methane to ethane and ethylene in the presence of oxygen at about 700 °C.[4−6] Second, the highly ionic character of the chemical bond in MgO makes these crystals tractable by current quantum mechanical methods,[7] thus making Li/MgO an ideal theoretical model for studying catalysis. Finally, a great deal of experimental and theoretical data has been compiled about point defects in MgO, including their electronic structure and chemical reactivity. Specifically, experimental studies on the reaction kinetics showed that hydrogen abstraction from methane over some reactive site on the Li/MgO surface is most likely to be the rate-limiting step in the conversion of methane to ethane.[8,9] The activation energy for such a reaction was reported in the range from 20 to 28 kcal/mol depending on the reaction conditions.[9,10] Although some role of surface F centers as active sites has been suggested,[11,12] numerous studies conclude that the surface O^- ion (or localized electronic hole) can be responsible for hydrogen abstraction. There are several possible modes of hole localization on the MgO surface discussed in the literature. Electronic holes may be self-trapped on the MgO-(001) surface[13] and additionally stabilized by the presence of Mg^{2+} vacancies[14,15] or in the low-coordinated sites.[13,16−19] In the bulk and on the surface of lithium-doped MgO, Li^+ ions occupy Mg^{2+} sites and stabilize the nearby O^- species resulting in $[Li^+O^-]$ defects.[15,20−24] Although theoretical studies suggest that $[Li^+O^-]$ defects can form aggregates,[25] the absence of spin exchange and dipolar broadening in the ESR spectra indicated that the $[Li^+O^-]$ centers must be well separated from one another by at least 8−10 Å.[20] At elevated reaction temperatures, electron holes can leave bulk Li^+ impurities, become localized on the surface, and thus increase the number of reactive centers.[1] However, the concentration and distribution of catalytic sites on the surface are unknown, and our understanding in regard to the mechanism of the entire catalytic cycle, including regeneration of the active site, is still incomplete at best.

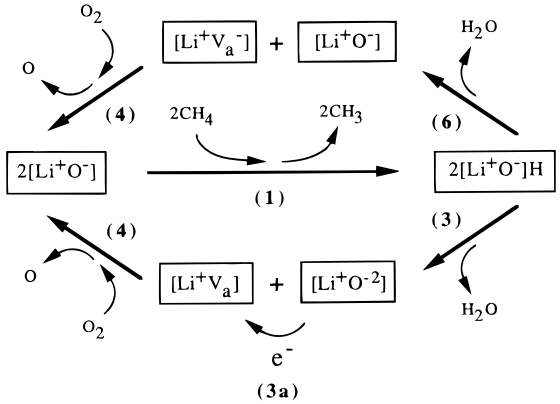

Figure 1. Two alternative cycles of the Ito−Lunsford mechanism. Both cycles begin with the two neighboring $[Li^+O^-]$ defects shown at the left followed by reaction 1. The lower channel involves proton migration between defects. The upper loop shows an analogous reaction with a mobile hydrogen atom.

To our knowledge, the only mechanism for the oxidative coupling of methane above the Li/MgO catalyst was proposed by Ito and Lunsford.[5,26] This mechanism is shown schematically in Figure 1. In this figure, and throughout the text, we commonly use notation in which brackets enclose the surface defect, and species indicated outside the brackets are adsorbates at the defect site. In more detail, the Ito−Lunsford mechanism implies participation of at least two trapped-hole $[Li^+O^-]$ surface defects and consists of three steps. The first step is hydrogen abstraction by $[Li^+O^-]$ defects with formation of two surface OH^- groups

$$2[Li^+O^-] + 2CH_4(g) \rightarrow 2[Li^+O^-]H + 2CH_3(g) \quad (1)$$

The resultant methyl radicals couple in the gas phase to form ethane

$$2CH_3(g) \rightarrow C_2H_6(g) \quad (2)$$

† On leave from the Institute of Chemical Physics, University of Latvia, 19 Rainis blvd, Riga LV1586, Latvia.
* Corresponding author.
⊗ Abstract published in *Advance ACS Abstracts,* April 1, 1997.

S1089-5647(97)00012-6 CCC: $14.00 © 1997 American Chemical Society

The second step involves dissociation of one surface OH^- group into a lattice O^{2-} ion and a mobile surface proton. This proton migrates to another OH^- to form a water molecule which desorbs from the surface, leaving behind an anion vacancy V_a. Thus, step two can be represented by the single equation

$$2[Li^+O^-]H \rightarrow [Li^+O^{2-}] + [Li^+V_a] + H_2O(g) \qquad (3)$$

The final step is regeneration of the active site, which involves electron transfer to the anion vacancy

$$[Li^+O^{2-}] + [Li^+V_a] \rightarrow [Li^+O^-] + [Li^+V_a^-] \qquad (3a)$$

and dissociative chemisorption of oxygen

$$[Li^+V_a^-] + O_2(g) \rightarrow [Li^+O^-] + O \qquad (4)$$

Thus, two iterations of the Ito−Lunsford cycle result in the following conversion

$$4CH_4(g) + O_2(g) \xrightarrow{Li/MgO} 2C_2H_6(g) + 2H_2O(g) \qquad (5)$$

While the Ito−Lunsford mechanism successfully incorporates hydrogen abstraction from methane and regeneration of the reactive center, certain features of this mechanism appear to be unlikely. First, it requires removal of a lattice oxygen from the lattice site which is expected to be highly endothermic. For example, theoretical estimates for the removal of an oxygen atom from the MgO(001) surface are well in excess of 170 kcal/mol.[13,27−29] Therefore, in contrast to experimental data, oxygen removal and not hydrogen abstraction would be the rate-limiting step in this catalytic cycle.[5] Second, migration of a proton, as in reaction 3, requires substantial energy to overcome a strong electrostatic attraction between oppositely charged species $[Li^+O^{2-}]$ and H_{ads}^+. Third, a large separation between $[Li^+O^-]$ centers implies a low probability for charge transfer (eq 3a) between defects.

The electron transfer step is not required if one considers hydrogen atom migration between defects[5] (see upper cycle in Figure 1)

$$2[Li^+O^-]H \rightarrow [Li^+V_a^-] + [Li^+O^-] + H_2O(g) \qquad (6)$$

instead of proton migration. However, hydrogen atom interactions with the nondefective MgO surface are very weak,[30−32] and at high temperatures desorption is expected instead of migration on the surface.

The above discussion of the Ito−Lunsford mechanism naturally leads to the following question: Is it possible to suggest a full cycle of catalytic surface reactions that (i) can proceed from only one $[Li^+O^-]$ active site and (ii) does not require the removal of surface lattice oxygen? On the basis of these conditions, and assuming such types of surface reactions as molecular or dissociative adsorption of oxygen, hydrogen abstraction from methane, and water desorption, we can formally suggest that conversion of methane over $[Li^+O^-]$ defects should proceed through several reaction intermediates with the general form

$$[Li^+O^-]O_nH_m \quad (n = 0, 1, 2; m = 0, 1, 2) \qquad (7)$$

This gives rise to three questions which we will address in the remainder of this paper: (1) Which species from eq 7 are stable and can serve as reaction intermediates? (2) Can the stable species participate in thermodynamically allowable reactions with gas phase molecules? (3) Is it possible to construct closed catalytic cycles from these reactions? To answer the above questions, we have performed *ab initio* calculations using an embedded cluster model of the $[Li^+O^-]$ active site at the MgO-(001) surface. This model and the computational techniques used are described in the next section.

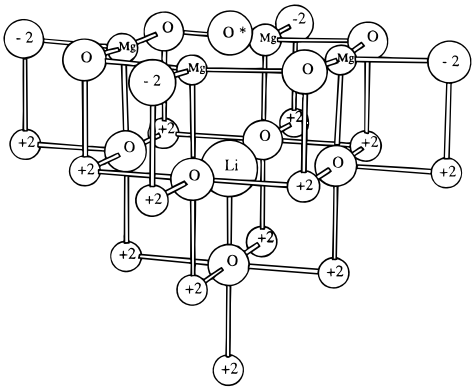

Figure 2. Optimized geometry for the $[Li^+O^-]$ surface defect. This cluster is embedded in the field generated by 224 additional point charges (not shown).

Computational Method

The strategy employed in this work is to first optimize geometries for the surface defects of eq 7 as well as other relevant species. From calculated total energies of stable intermediates, we determine reaction energies for different possible catalytic cycles. This information can tell us about the relative importance of different reaction channels. Although information about transition states is required for a thorough characterization of reactions, we leave the identification of transition states for our future work.

The embedded cluster model used here is similar to that employed in our previous study.[32] We used the cluster shown in Figure 2 to model adsorption at the $[Li^+O^-]$ defect. We have placed the Li^+ ion in the second layer of the MgO(001) surface. This choice is somewhat arbitrary, and it would be interesting to investigate the dependence of results on position of the lithium impurity. However, as discussed above, we believe that the role of lithium is merely to stabilize the main reactive species O^-; therefore, the impurity position is of secondary importance.

In the energy minimization procedures, all adsorbate atoms, the reactive surface oxygen (marked as O* in Figures 2 and 3), and its nearest magnesium neighbors were fully relaxed with no elements of symmetry assumed. Lithium was allowed to move normal to the surface, and all other ions were held fixed at ideal lattice positions. Several trial configurations were considered for each adsorbate of eq 7. Some optimized adsorbate structures are shown in Figure 3 where only the central part of the cluster is depicted.

Depending on multiplicity, geometry optimizations were performed by using either the restricted or restricted open-shell Hartree−Fock methods. For computational feasibility, ionic cores were approximated by Stevens−Basch−Krauss compact effective pseudopotentials (CEP).[33] We used the standard valence CEP-31G** basis set on lithium, on the central oxygen atom, and on all adsorbed atoms. The CEP-31G basis set was used for nine oxygen ions nearest to the Li^+-O^* pair. Oxygen ions marked as "−2" in Figure 2 were modeled as point charges without basis functions. The CEP-4G basis set was placed on the four Mg ions at the surface, and for a better description of the interaction between these ions and their oxygen neighbors modeled as point charges, short-range classical repulsions[34] between these centers were added to the total energy of the cluster. Without this repulsive potential, Mg ions would simply collapse on their point-charge neighbors. Other Mg ions in the

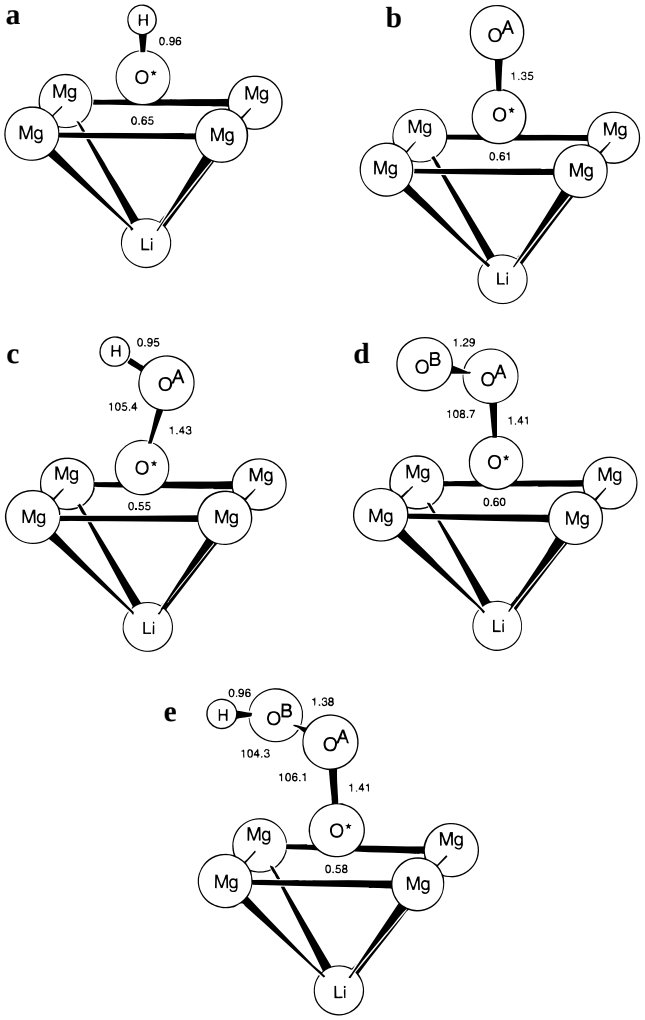

Figure 3. Optimized geometries of selected surface species. Only the central part of the cluster in Figure 2 is shown. Bond lengths and the height of the O* atom above the surface are in angstroms; bond angles are in degrees. (a) $[Li^+O^-]H$, (b) $[Li^+O^-]O$, (c) $[Li^+O^-]OH$, (d) $[Li^+O^-]O_2$, (e) $[Li^+O^-]O_2H$.

TABLE 1: Bond Energies (kcal/mol) for Some Gas Phase Molecules and Reaction Energy for Methane Conversion to Ethane (See Eq 5)

equation	HF	MP2	expt
$O_2 \rightarrow O + O$	22	113	119.106 ± 0.048^a
$H_2O \rightarrow OH + H$	89	119	119 ± 1^a
$OH \rightarrow O + H$	68	96	102.3 ± 0.5^a
$CH_4 \rightarrow CH_3 + H$	88	107	104 ± 1^a
$C_2H_6 \rightarrow CH_3 + CH_3$	67	92	88 ± 2^a
$4CH_4 + O_2 \rightarrow 2C_2H_6 + 2H_2O$	−74	−73	-84.5^b

[a] D°_{298}, ref 48. [b] ΔHf°_{298}, ref 48.

cluster (labeled "+2") were approximated by bare pseudopotentials without basis sets. We describe a surface anion vacancy by removing the central oxygen core while leaving its basis set in the vacancy. This is common practice when an accurate representation of the electron distribution in the V_a^- defect (F^+ center) is required.[28]

Correlation energy was included by performing single-point second-order Møller−Plesset perturbation theory (MP2) calculations at Hartree−Fock optimized geometries. As an indication of the quality of our chosen correlation method, pseudopotential, and basis sets, we compare in Table 1 the calculated bond energies of relevant gas phase molecules with experimental data. Note the significant improvement of MP2 results as compared to Hartree−Fock calculations.

In order to represent the rest of the crystal, the cluster described above was embedded in the field generated by 224 lattice point charges of ±2. For a better view of the active site, the entire system is not shown in Figure 2. It consisted of four stacked 8 × 8 layers resulting in an 8 × 8 × 4 slab. This finite lattice has been shown to provide an accurate Madelung potential at the (001) rock salt crystal surface.[32]

Although it is known that crystal polarization can have a significant effect on calculated energies of charged defects,[23,35] our model does not allow for polarization in the lattice surrounding the $[Li^+O^-]$ defect. Since most of the defects considered here are neutral, and we calculate relative energies rather than absolute values, we expect errors from such neglect of lattice polarization to be small.

All calculations were performed using the GAUSSIAN-92 computer code[36] that was modified to include analytical first derivatives of interactions between ions in the quantum cluster and the lattice of point charges.

In characterizing the electronic structure of various surface defects, we present results for the electronic density of states (DOS). These DOS graphs were generated by Gaussian smoothing of orbital energy levels with the exponent of 440 hartree^{-2}. Although these graphs do not take into account electron correlation effects, DOS information can be useful for qualitative analysis of data collected in surface characterization experiments.[37]

Results

$[Mg^{2+}O^{2-}]$. This cluster models the regular MgO(001) surface. Optimized positions of lattice ions do not deviate significantly from ideal lattice sites. Mg^{2+} surface ions move slightly toward the bulk, and oxygen relaxes away from the surface by 0.06 Å. Such small relaxations are in qualitative agreement with existing experimental data and other accurate calculations.[27] This further supports the quality of our cluster model and computational methods. The calculated DOS is depicted by the solid line in Figure 4a and provides a base-line comparison to more complicated defect structures.

$[Li^+O^-]$. In our calculations, the electronic hole is well localized on the surface O* oxygen atom. Almost 98% of the electron spin density is concentrated on the p_z orbital of this atom. The optimized geometry for a lithium-trapped hole defect is shown in Figure 2. The O* atom relaxes away from the surface by 0.35 Å, and the Li^+ ion moves toward the bulk so that the Li^+-O^* spacing is increased by 0.53 Å with respect to the $[Mg^{2+}O^{2-}]$ cluster. This agrees qualitatively with both theoretical and experimental studies of bulk defects,[23,38,39] although a contraction of the defect bond distance has also been calculated.[24] The DOS for the $[Li^+O^-]$ defect is compared with that of the regular MgO(001) surface in Figure 4a. Due to the reduced electrostatic potential on oxygen ions close to the Li^+ impurity, their energy levels are higher. This causes the broadening of the "valence bands" clearly seen in Figure 4a. A half-filled $O^*_{p_z}$ level splits into the band gap, and a shoulder appears on the lower part of the valence band due to $O^*_{p_{xy}}$ levels.

$[Li^+O^{2-}]$ and $[Li^+V_a]$. In comparison to the $[Mg^{2+}O^{2-}]$ structure, the O* atom of a closed-shell $[Li^+O^{2-}]$ defect moves to a height of 0.33 Å above the surface, and the cation is displaced in the direction of the bulk. This results in an Li^+-O^* spacing that is increased by 0.40 Å over the $[Mg^{2+}O^{2-}]$ cluster. The major differences in the DOS of $[Li^+O^{2-}]$ with respect to $[Mg^{2+}O^{2-}]$ are a band broadening and a uniform shift to higher energies due to the reduced charge of the cation. In contrast, the DOS structure of the positively charged $[Li^+V_a]$ is shifted to lower energies in comparison to $[Mg^{2+}O^{2-}]$.

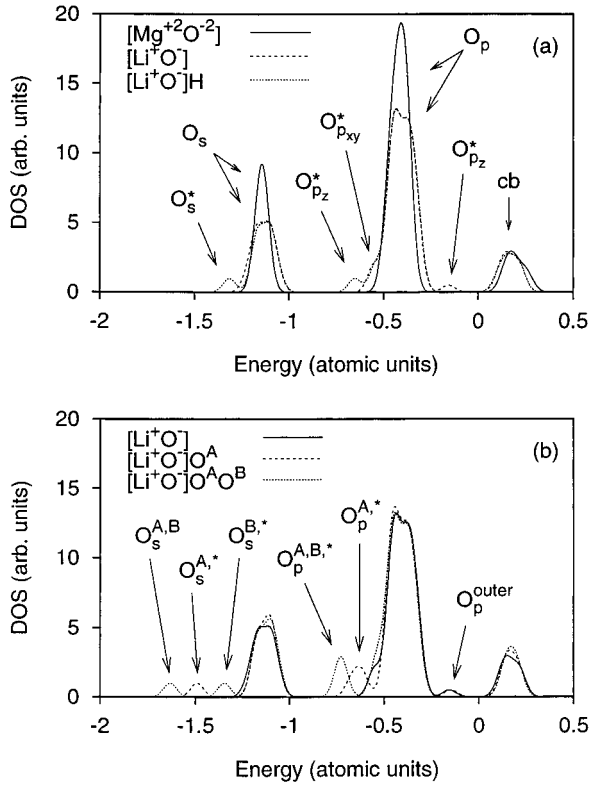

Figure 4. Calculated DOS. For atom labeling; see Figure 3. The conduction band states are labeled "cb", and "outer" refers to the single oxygen atom (O*, O^A, or O^B) that is farthest away from Li^+. (a) Comparison of the MgO(001) surface (solid line) with the $[Li^+O^-]$ (dashed line) and the $[Li^+O^-]H$ (dotted line) defects. (b) Comparison of the various stages of oxygen chemisorption at the $[Li^+O^-]$ defect.

$[Li^+V_a^-]$. An electron trapped in an oxygen vacancy (V_a^-) is analogous to an F^+ center. Our calculations show that four neighboring surface Mg^{2+} ions relax laterally outward by an average of 0.09 Å. This is consistent with other theoretical studies.[28,40] We found the position of the defect level to be about 7.6 eV above the top of the valence band. This is much higher than that reported in refs 28 and 40 for F^+ centers because Li^+ substituting for Mg^{2+} decreases the electrostatic potential in the vacancy by several electronvolts. For the same reason, the energy required to remove oxygen from the $[Li^+O^-]$ defect (118 kcal/mol in our calculations) to form $[Li^+V_a^-]$ and O(g) is lower than the energy to remove an oxygen atom from the ideal MgO(001) surface. Theoretical estimates for the latter range from 177 to 229 kcal/mol.[27−29]

$[Li^+O^-]H$. Properties of OH^- ions associated with bulk Li^+ impurities are documented in literature.[41] Shown in Figure 3a is the relaxed geometry of surface $[Li^+O^-]H$. Our calculated O*−H bond distance of 0.96 Å agrees exactly with the OH^- gas phase value.[42] In Figure 4a we illustrate the effects of adsorbed hydrogen on the density of states of the $[Li^+O^-]$ defect. The defect level in the band gap is removed, and additional peaks appear on the lower energy side of both O_s and O_p valence bands. The hydrogen affinity of 121 kcal/mol (see Table 2) is larger than the C−H bond energy in methane, which is 107 kcal/mol in our calculations (see Table 1). This confirms the role of surface $[Li^+O^-]$ defects as active sites for hydrogen abstraction from methane.

$[Li^+O^-]O$ and $[Li^+O^-]OH$. Atomic oxygen chemisorbed to the $[Li^+O^-]$ defect yields a surface species similar to superoxide ion, O_2^-. Our calculated bond length of 1.35 Å for O^*-O^A (see Figure 3b) is very close to the 1.34 Å reported for superoxide ion in the gas phase.[42] In comparison to $[Li^+O^-]$, the DOS of $[Li^+O^-]O$ (Figure 4b) has additional features in the lower energy parts of both O_s and O_p valence bands. They are associated with O* and O^A oxygen atoms. The half-filled band gap state produced by the surface superoxide ion lies very close to that of the $[Li^+O^-]$ defect. However, in the former case, this state and the maximum of the spin density distribution are associated with the adsorbed (outer) oxygen O^A. This indicates that adsorbed oxygen is now the reactive center. We have found a large hydrogen affinity of $[Li^+O^-]O$ (93 kcal/mol, see Table 2) and a stable configuration of the diamagnetic $[Li^+O^-]OH$ defect (Figure 3c) in our calculations. This agrees with experimental evidence that superoxide ion can be stable on the surface of MgO crystals and abstract hydrogen from methane.[43] Similar to $[Li^+O^-]H$, addition of hydrogen to superoxide results in removal of the band gap state and a splitting of the feature in the lower energy part of the O_p band into two peaks.

$[Li^+O^-]O_2$ and $[Li^+O^-]O_2H$. In studying adsorption of molecular oxygen at the $[Li^+O^-]$ site, we found a local minimum corresponding to the paramagnetic $[Li^+O^-]O_2$ species (Figure 3d) resembling an ozonide ion. In this metastable state, molecular oxygen has a negative binding energy (−9 kcal/mol, see Table 2) to the surface. Ozonide ions have been experimentally detected on the surface of MgO at temperatures below 150 °C.[44] Similar to both $[Li^+O^-]$ and $[Li^+O^-]O$ defects, adsorbed diatomic oxygen gives rise to an electronic state in the band gap, and the related spin density is concentrated on the outermost oxygen atom (O^B). Additional features appear below the O_s and O_p valence bands as shown in Figure 4b. The effect of hydrogen adsorption to this system is similar to that discussed above for the $[Li^+O^-]O$ defect. A singlet state $[Li^+O^-]O_2H$ defect is produced which cannot be detected using ESR techniques. Our calculated value for the hydrogen affinity of $[Li^+O^-]O_2$ is 88 kcal/mol. This indicates a substantial reactivity of this defect in agreement with experimental observations for ozonide ion on the MgO surface.[44]

$[Li^+O^-]H_2$, $[Li^+O^-]OH_2$, and $[Li^+O^-]O_2H_2$. We were not able to find stable configurations for hydrogen, water, and hydrogen peroxide adsorbed at the $[Li^+O^-]$ defect. All initial geometries for adsorbed molecular hydrogen dissociated into $[Li^+O^-]H$ and gas phase atomic hydrogen. It seems that the only way to bind atomic hydrogen to $[Li^+O^-]H$ is to first remove the OH group sufficiently far from the surface. This results in a gas phase water molecule and the $[Li^+V_a^-]$ defect on the surface as in eq 6 of the Ito−Lunsford mechanism.

TABLE 2: Calculated MP2 Binding Energies (kcal/mol) for Adsorbates Related to the Oxidative Coupling of Methane Over Li/MgO and Results for Similar Systems Taken from Literature

surface	adsorbate	binding energy	results from lit.
$[Li^+V_a^-]$	O	118	225[a]
$[Li^+O^-]$	H	121	107[b]
$[Li^+O^-]$	O	54	40[c]
$[Li^+O^-]$	O_2	−9	
$[Li^+O^-]$	OH	51	56[d]
$[Li^+O^-]$	O_2H	40	
$[Li^+O^-]O$	H	93	63[e]
$[Li^+O^-]O$	O	50	58[f]
$[Li^+O^-]O$	OH	42	
$[Li^+O^-]O_2$	H	88	

[a] Energy required to remove an O atom from the MgO(001) surface lattice site in ref 27. Other estimates include 177 from ref 28 and 229 from ref 29. [b] From ref 15. [c] For oxygen atom adsorption to O^- on MgO in ref 49. [d] ΔE for $O_2H^-(g) \rightarrow O^-(g) + OH(g)$ determined using the electron affinities of O_2H and O from ref 50, calculated O_2-H bond energy from ref 51, and experimental bond energies of O_2 and OH from ref 48. [e] ΔE for $O_2H^-(g) \rightarrow O_2^-(g) + H(g)$ determined using the electron affinities of O_2H and O_2 from ref 50 and the calculated O_2-H bond energy from ref 51. [f] ΔE for $O_3^-(g) \rightarrow O_2^-(g) + O(g)$ determined using the calculated atomization energy of O_3^- from ref 52 and the O_2^- bond energy taken from ref 42.

TABLE 3: Calculated Reaction Energies (kcal/mol) for Processes Related to the Ito−Lunsford Mechanism[a]

eq no.	reaction	ΔE^{MP2}
(1)	$2[Li^+O^-] + 2CH_4(g) \rightarrow 2[Li^+O^-]H + 2CH_3(g)$	−28
(3)	$2[Li^+O^-]H \rightarrow [Li^+O^{2-}] + [Li^+V_a] + H_2O(g)$	+162
(3a)	$[Li^+O^{2-}] + [Li^+V_a] \rightarrow [Li^+O^-] + [Li^+V_a^-]$	−17
(4)	$[Li^+V_a^-] + O_2(g) \rightarrow [Li^+O^-] + O(g)$	−5
(4a)	$[Li^+V_a^-] + O(g) \rightarrow [Li^+O^-]$	−118
(6)	$2[Li^+O^-]H \rightarrow [Li^+V_a^-] + [Li^+O^-] + H_2O(g)$	+145
(8)	$[Li^+O^-]H + H(g) \rightarrow [Li^+V_a^-] + H_2O(g)$	+24

[a] A cycle composed of reactions 1−4a is shown graphically in Figure 5a.

Although the endothermicity of the reaction

$$[Li^+O^-]H + H(g) \rightarrow [Li^+V_a^-] + H_2O(g) \qquad (8)$$

is only 24 kcal/mol, it most likely has a large activation barrier. Although we have not found a stable structure for $[Li^+O^-]OH_2$, our results suggest that water can either form a weakly bound complex with the surface $[Li^+O^-]$ defect or undergo dissociation into gas phase OH and an adsorbed hydrogen atom.[45] We found that, depending on initial geometry, adsorbed O_2H_2 dissociates according to one of the following schemes

$$[Li^+O^-]OHOH \rightarrow [Li^+O^-]OH + OH(g)$$

$$[Li^+O^-]OOH_2 \rightarrow [Li^+O^-]O + H_2O(g)$$

Discussion

In our calculations, the overall conversion shown in eq 5 is exothermic by 73 kcal/mol. This conversion can be achieved through several different cycles of surface reactions. On the basis of computed energies of the stable surface reaction intermediates presented in the previous section, we can construct energy profiles for these catalytic cycles.

Reaction energies for the surface processes that compose the Ito−Lunsford cycle appear in Table 3, and the proton transfer channel is diagrammed in Figure 5a. As already mentioned in the Introduction, oxygen removal from the lattice site requires a large amount of energy; our calculations yield 162 and 145 kcal/mol for reactions 3 and 6, respectively. These are well in excess of the experimentally determined activation energy for methane conversion, which is about 55 kcal/mol.[5,46]

Considering the results of our calculations, we have assembled in Figure 6 the collection of possible catalytic cycles that satisfy conditions (i) and (ii) from the introduction. The hydrogen abstraction reaction

$$[Li^+O^-] + CH_4(g) \rightarrow [Li^+O^-]H + CH_3(g) \qquad \Delta E = -14 \text{ kcal/mol} \quad (9)$$

is exothermic, but all other surface reactions shown in Figure 6 with thin arrows, and listed in the lower portion of Table 4, have positive reaction energies in excess of 40 kcal/mol. Therefore, we focus our discussion on the cycle indicated by bold arrows in Figure 6. This cycle begins with adsorption of molecular oxygen on the $[Li^+O^-]$ defect, resulting in the formation of a surface ozonide ion (eq 10 of Table 4). This species abstracts hydrogen from methane forming another stable intermediate $[Li^+O^-]O_2H$, which, in its turn, reacts with methane to form the $[Li^+O^-]O$ defect, a CH_3 radical, and a water molecule (see eq 12 of Table 4). As discussed in the previous section, $[Li^+O^-]O$ has a significant hydrogen affinity; therefore, it may abstract hydrogen from methane (eq 13 of Table 4) and then participate in a second reaction with methane to form water and restore the active site (eq 14 of Table 4). Positive energies

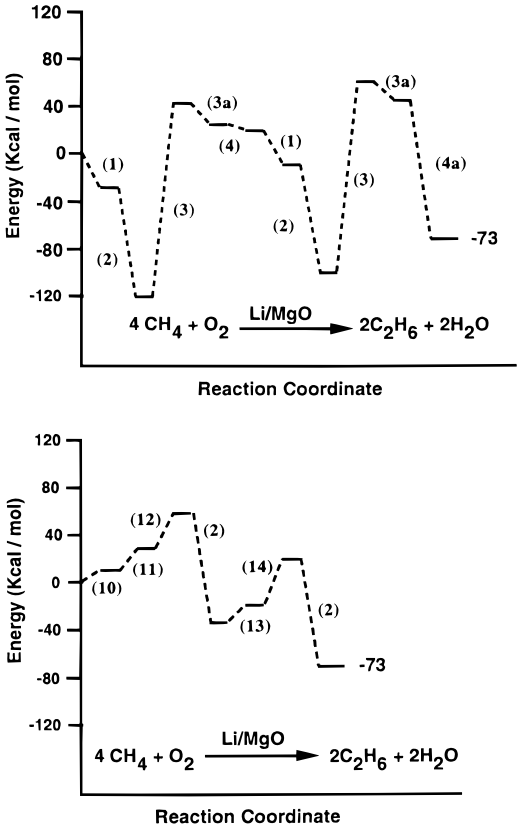

Figure 5. Calculated energy profiles for the methane conversion given by eq 5. Reaction numbers are given in parentheses. (a, top) Two iterations of the Ito−Lunsford cycle with proton transfer (see Table 3 for reaction energies). (b, bottom) Our proposed single site cycle indicated by bold arrows in Figure 6 (see Table 4 for reaction energies).

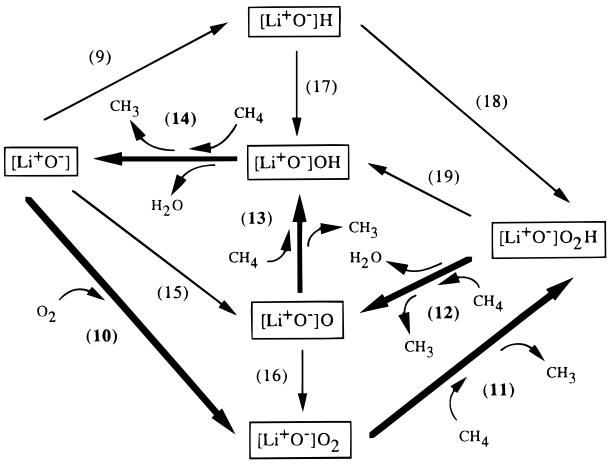

Figure 6. Possible catalytic cycles that involve only one $[Li^+O^-]$ reactive site. All reaction energies are given in Table 4. The cycle shown by bold arrows is discussed in the text and illustrated in the energy profile of Figure 5b.

of surface reactions in Table 4 are compensated by exothermic coupling of gas phase methyl radicals (reaction 2).

Since the cycle indicated by bold arrows in Figure 6 leads to the overall conversion given in eq 5, it can be conveniently compared with a 2-fold iteration of the Ito−Lunsford mechanism. In our proposed cycle, the largest endothermicities (14−39 kcal/mol) are for hydrogen abstraction steps (see Figure 5b). Although we have no information about the reaction barriers, these calculated energy changes suggest that hydrogen abstraction is likely to be the rate-limiting step in our mechanism. This is qualitatively consistent with experimental evidence discussed in the Introduction and differs from the Ito−Lunsford mecha-

TABLE 4: Calculated Reaction Energies (kcal/mol) for Processes Shown in Figure 6[a]

eq no.	reaction	ΔE^{MP2}
(10)	$[Li^+O^-] + O_2(g) \rightarrow [Li^+O^-]O_2$	+9
(11)	$[Li^+O^-]O_2 + CH_4(g) \rightarrow [Li^+O^-]O_2H + CH_3(g)$	+19
(12)	$[Li^+O^-]O_2H + CH_4(g) \rightarrow [Li^+O^-]O + H_2O(g) + CH_3(g)$	+30
(13)	$[Li^+O^-]O + CH_4(g) \rightarrow [Li^+O^-]OH + CH_3(g)$	+14
(14)	$[Li^+O^-]OH + CH_4(g) \rightarrow [Li^+O^-] + H_2O(g) + CH_3(g)$	+39
(9)	$[Li^+O^-] + CH_4(g) \rightarrow [Li^+O^-]H + CH_3(g)$	−14
(15)	$[Li^+O^-] + O_2(g) \rightarrow [Li^+O^-]O + O(g)$	+59
(16)	$[Li^+O^-]O + O_2(g) \rightarrow [Li^+O^-]O_2 + O(g)$	+63
(17)	$[Li^+O^-]H + O_2(g) \rightarrow [Li^+O^-]OH + O(g)$	+87
(18)	$[Li^+O^-]H + O_2(g) \rightarrow [Li^+O^-]O_2H$	+42
(19)	$[Li^+O^-]O_2H + CH_4(g) \rightarrow [Li^+O^-]OH + OH(g) + CH_3(g)$	+56

[a] Our proposed cycle for the oxidative coupling of methane over Li/MgO is composed of reactions 10−14. Its energy profile is shown in Figure 5b.

nism where the lattice oxygen removal step is most likely to be rate limiting.

In calculating energies for reactions 15−17 in Table 4, we assumed that an oxygen atom is released into the gas phase. Adsorption of this species on the MgO surface may result in an energy gain of about 40 kcal/mol,[47] thus substantially reducing the endothermicities of reactions 15−17 and making additional catalytic channels energetically comparable with the cycle discussed above. Although a complicated dynamical chemical equilibrium exists at the elevated temperatures required for operation of the Li/MgO catalyst, we believe that the single-site catalytic cycle presented here is credible and perhaps competes with the Ito−Lunsford cycle for production of methyl radicals at the catalyst surface.

Conclusions

Using an *ab initio* embedded cluster model, we have systematically examined the structure and stability of various defects on the Li-doped MgO(001) surface. From these results, we propose a new catalytic cycle for the oxidative coupling of methane that involves only one defect site. This newly proposed cycle differs significantly from the existing Ito−Lunsford mechanism which requires exchange of a proton and an electron between two distant defect sites and the energetically unfavorable process of lattice oxygen removal. Our calculations predict that, in addition to the well-known $[Li^+O^-]$ defect, other surface species such as $[Li^+O^-]O_2$ and $[Li^+O^-]O$ may abstract hydrogen from methane. Our proposed catalytic cycle is supported by experimental results regarding the rate-limiting step and activation energy for methane conversion to ethane.

Acknowledgment. This research was supported by the University of Utah and the National Science Foundation through a NSF Young Investigator Award to T.N.T.

References and Notes

(1) Lunsford, J. H. *Catal. Today* **1990**, *6*, 235.
(2) Crabtree, R. H. *Chem. Rev.* **1995**, *95*, 987.
(3) Lunsford, J. H. *Angew. Chem., Int. Ed. Engl.* **1995**, *34*, 970.
(4) Hutchings, G. J.; Woodhouse, J. R.; Scurrell, M. S. *J. Chem. Soc., Faraday Trans. 1* **1989**, *85*, 2507.
(5) Ito, T.; Wang, J.-X.; Lin, C.-H.; Lunsford, J. H. *J. Am. Chem. Soc.* **1985**, *107*, 5062.
(6) Keller, G. E.; Bhasin, M. M. *J. Catal.* **1982**, *73*, 9.
(7) Grimes, R. W., Catlow, C. R. A., Shluger, A. L., Eds. *Quantum Mechanical Cluster Calculations in Solid State Studies*; World Scientific: Singapore, 1992.
(8) Cant, N. W.; Lukey, C. A.; Nelson, P. F.; Tyler, R. J. *J. Chem. Soc., Chem. Commun.* **1988**, 766.
(9) Amorebieta, V. T.; Colussi, A. J. *J. Phys. Chem.* **1988**, *92*, 4576.
(10) Campbell, K. D.; Lunsford, J. H. *J. Phys. Chem.* **1988**, *92*, 5792.
(11) Wu, M.-C.; Truong, C. M.; Coulter, K.; Goodman, D. W. *J. Am. Chem. Soc.* **1992**, *114*, 7565.
(12) Wu, M.-C.; Truong, C. M.; Coulter, K.; Goodman, D. W. *J. Catal.* **1993**, *140*, 344.
(13) Shluger, A. L.; Grimes, R. W.; Catlow, C. R. A.; Itoh, N. *J. Phys.: Condens. Matter* **1991**, *3*, 8027.
(14) Pope, S. A.; Guest, M. F.; Hillier, I. H.; Colbourn, E. A.; Mackrodt, W. C.; Kendrick, J. *Phys. Rev. B* **1983**, *28*, 2191.
(15) Børve, K. J.; Pettersson, L. G. M. *J. Phys. Chem.* **1991**, *95*, 7401.
(16) Børve, K. J. *J. Chem. Phys.* **1991**, *95*, 4626.
(17) Kobayashi, H.; Salahub, D. R.; Ito, T. *J. Phys. Chem.* **1994**, *98*, 5487.
(18) Shluger, A. L.; Gale, J. D.; Catlow, C. R. A. *J. Phys. Chem.* **1992**, *96*, 10389.
(19) Anpo, M.; Doi, T.; Matsuura, I.; Sunamoto, M. *Chem. Lett.* **1988**, 701.
(20) Wang, J.-X.; Lunsford, J. H. *J. Phys. Chem.* **1986**, *90*, 5883.
(21) Abraham, M. M.; Chen, Y.; Boatner, L. A.; Reynolds, R. W. *Phys. Rev. Lett.* **1976**, *37*, 849.
(22) Chen, Y.; Tohver, H. T.; Narayan, J.; Abraham, M. M. *Phys. Rev. B* **1977**, *16*, 5535.
(23) Shluger, A. L.; Kotomin, E. A.; Kantorovich, L. N. *J. Phys. C: Solid State Phys.* **1986**, *19*, 4183.
(24) Zuo, J.; Pandey, R.; Kunz, A. B. *Phys. Rev. B: Condens. Matter* **1991**, *44*, 7187.
(25) Foot, J. D.; Colbourn, E. A.; Catlow, C. R. A. *J. Phys. Chem. Solids* **1988**, *49*, 1225.
(26) Driscoll, D. J.; Martir, W.; Wang, J.-X.; Lunsford, J. H. *J. Am. Chem. Soc.* **1985**, *107*, 58.
(27) Kantorovich, L. N.; Holender, J. M.; Gillan, M. J. *Surf. Sci.* **1995**, *343*, 221.
(28) Ferrari, A. M.; Pacchioni, G. *J. Phys. Chem.* **1995**, *99*, 17010.
(29) Castanier, E.; Noguera, C. *Surf. Sci.* **1996**, *364*, 1.
(30) Ito, T.; Sekino, T.; Moriai, N.; Tokuda, T. *J. Chem. Soc., Faraday Trans. 1* **1981**, *77*, 2181.
(31) Ito, T.; Kuramoto, M.; Yoshioka, M.; Tokuda, T. *J. Phys. Chem.* **1983**, *87*, 4411.
(32) Stefanovich, E. V.; Truong, T. N. *J. Chem. Phys.* **1995**, *102*, 5071.
(33) Stevens, W. J.; Basch, H.; Krauss, M. *J. Chem. Phys.* **1984**, *81*, 6026.
(34) Pandey, R.; Zuo, J.; Kunz, A. B. *J. Mater. Res.* **1990**, *5*, 623.
(35) Vail, J. M.; Harker, A. H.; Harding, J. H.; Saul, P. *J. Phys. C: Solid State Phys.* **1984**, *17*, 3401.
(36) Frisch, M. J.; Trucks, G. W.; Schlegel, H. B.; Gill, P. M. W.; Johnson, B. G.; Wong, M. W.; Foresman, J. B.; Robb, M. A.; Head-Gordon, M.; Replogle, E. S.; Gomperts, R.; Andres, J. L.; Raghavachari, K.; Binkley, J. S.; Gonzalez, C.; Martin, R. L.; Fox, D. J.; Defrees, D. J.; Baker, J.; Stewart, J. J. P.; Pople, J. A. *Gaussian 92/DFT, Revision G.3*; Gaussian, Inc.: Pittsburgh, PA, 1993.
(37) Ochs, D.; Maus-Friedrichs, W.; Brause, M.; Günster, J.; Kempter, V.; Puchin, V.; Shluger, A.; Kantorovich, L. *Surf. Sci.* **1996**, *365*, 557.
(38) Shluger, A. L.; Heifets, E. N.; Gale, J. D.; Catlow, C. R. A. *J. Phys.: Condens. Matter* **1992**, *4*, 5711.
(39) Abraham, M. M.; Unruh, W. P.; Chen, Y. *Phys. Rev. B* **1974**, *10*, 3540.
(40) Eglitis, R. I.; Kuklja, M. M.; Kotomin, E. A.; Stashans, A.; Popov, A. I. *Comput. Mater. Sci.* **1996**, *5*, 298.
(41) González, R.; Pareja, R.; Chen, Y. *Phys. Rev. B* **1992**, *45*, 12730.
(42) JANAF Thermochemical Tables, *J. Phys. Chem. Ref. Data*. **1985** (Suppl. 1).
(43) Iwamoto, M.; Lunsford, J. H. *J. Phys. Chem.* **1980**, *84*, 3079.
(44) Takita, Y.; Lunsford, J. H. *J. Phys. Chem.* **1979**, *83*, 683.
(45) Hewett, K. B.; Anderson, L. C.; Rosynek, M. P.; Lunsford, J. H. *J. Am. Chem. Soc.* **1996**, *118*, 6992.
(46) Coulter, K.; Goodman, D. W. *Catal. Lett.* **1992**, *16*, 191.
(47) Kantorovich, L. N.; Gillan, M. J. *Surf. Sci.*, in press.
(48) Weast, R. C., Astle, M. J., Eds. *CRC Handbook of Chemistry and Physics*, 62nd ed.; CRC Press: Boca Raton, FL, 1981−1982.
(49) Nygren, M. A.; Pettersson, L. G. M. *Chem. Phys. Lett.* **1994**, *230*, 456.
(50) Huheey, J. E.; Keiter, E. A.; Keiter, R. L. *Inorganic Chemistry: Principles of Structure and Reactivity*; Harper Collins: New York, 1993; pp 42−43.
(51) Bauschlicher Jr., C. W.; Partridge, H. *Chem. Phys. Lett.* **1993**, *208*, 241.
(52) Borowski, P.; Roos, B. O.; Racine, S. C.; Lee, T. J.; Carter, S. *J. Chem. Phys.* **1995**, *103*, 266.